Catalysis Today 165 (2011) 19–24

Contents lists available at ScienceDirect

Catalysis Today

journal homepage: www.elsevier.com/locate/cattod

A density functional theory study of small Au nanoparticles at CeO_2 surfaces

Wen-Jun Zhu, Jie Zhang, Xue-Qing Gong*, Guanzhong Lu*

Labs for Advanced Materials, Research Institute of Industrial Catalysis, East China University of Science and Technology, 130 Meilong Road, Shanghai 200237, PR China

ARTICLE INFO

Article history:
Received 10 September 2010
Received in revised form
18 November 2010
Accepted 29 November 2010
Available online 7 January 2011

Keywords:
DFT + U
CeO_2
Gold catalysis
Three way catalysis
O_2 adsorption

ABSTRACT

Density functional theory calculations corrected for on-site Coulomb interactions (DFT + U) have been performed to study supported rare earth catalysts with small Au nanoclusters (Au trimer, Au_3) adsorbed at CeO_2 surfaces. The interaction of Au_3 with all the three major facets of crystalline CeO_2, namely CeO_2(1 1 1), (1 1 0) and (1 0 0), were systematically investigated. The results showed that Au_3 can adsorb rather strongly at the surfaces (E_{ads} > 3 eV), and partially reduce the CeO_2 support by filling the originally empty 4*f* orbital of one surface Ce with an electron. Moreover, corresponding to different configurations of surface relaxation caused by Au_3 adsorption, the localized 4*f* electron can occur at different surface Ce near the Au_3 at each surface. By calculating adsorption of O_2, we also showed that only the surface Ce at Au_3/CeO_2(1 1 0) are capable of strongly holding and activating the O_2.

1. Introduction

Cerium dioxide (Ceria, CeO_2) supported gold catalysts have recently attracted intensive research interest. This is primarily due to their excellent activity in promoting various reactions, such as low-temperature CO oxidation [1,2] and water–gas-shift reactions [3–5] that find important applications in vehicle emission control and energy production. In addition, as the main components of the catalysts, both CeO_2 and nanosized gold have also received very wide attention; (i) CeO_2 has long been used as the key intergradient in three-way-catalysts (TWC) for emission control, and due to the existence of unique localized 4*f* orbital, the electronic structures of CeO_2 related materials are also believed to determine their catalytic activities [6,7]; (ii) after Haruta and co-workers found that the 'noble' gold can be actually very active in catalytic reactions in the form of supported nanoparticles [8], lots of efforts have been devoted to illustrating the origins of Au catalysis [9–11], though issues such as the nature of active sites, the origin of size dependence effect and the stability of supported Au catalysts are still largely unsolved.

In one early theoretical work, Liu et al. [12] investigated single Au atom adsorbed at the CeO_2(111) surface by performing DFT calculations. They proposed that Au adatom is oxidized and the electron transferred from it to the surface is exclusively localized in the 4*f* orbital of a neighboring surface Ce cation. Several recent experimental and theoretical studies also showed that there exists $Au^{\delta+}$ species in the systems with small Au clusters adsorbed at CeO_2(1 1 1), and at the same time, a partial $Ce^{4+} \rightarrow Ce^{3+}$ reduction was also detected as some 4*f* orbitals were filled with electrons [13,14]. Moreover, clustering of Au nanoparticles at CeO_2 and the mechanisms of related catalytic reactions have also been studied by different experimental and theoretic approaches. Chen et al. [15] calculated the adsorption of single Au atom on the stoichiometric CeO_2(1 1 1) and CeO_2(1 1 0) surfaces and those with O or Ce vacancy. They determined that the stability of Au adsorption follows the order: Au/Ce-vacancy > Au/O-vacancy > Au/stoichiometric surface. They also showed that Au atom adsorption on a Ce-vacancy can cause large structural distortion to the surfaces and turn the surface O near the Au adatom to be more reactive compared to those of stoichiometric surfaces. Zhang et al. [16] compared the Au atom adsorption at various sites of CeO_2(1 1 1) and proposed that it prefers the O vacancy site rather than the stoichiometric surface site or Ce vacancy site, and therefore Au at O vacancy could be the centre for Au nucleation. Using scanning tunneling microscopy (STM) and other spectroscopy techniques, Weststrate [17] and Shaikhutdinov [18] and their co-workers also showed that O vacancies at CeO_2(1 1 1) can facilitate the adsorption and dispersion of small Au clusters. On the other hand, with DFT + U calculations, Camellone and Fabris [19] suggested that Au at Ce vacancy, or $Au_xCe_{1-x}O_2$ solid solutions, are in fact the active phase in catalytic low-temperature CO oxidation.

Despite the progress made in exploring the structural and electronic properties of different Au/CeO_2(1 1 1) systems, consensus regarding the origin of the catalytic activities and the unique role of the rare earth species and its localized 4*f* orbitals/electrons in the catalytic performance are still not reached. It should also be noted that CeO_2 materials in real use are usually in the form of nanocrystalline and besides (1 1 1), (1 1 0) and (1 0 0) are the major

* Corresponding authors.
E-mail addresses: xgong@ecust.edu.cn (X.-Q. Gong), gzhlu@ecust.edu.cn (G. Lu).

0920-5861/$ – see front matter © 2010 Elsevier B.V. All rights reserved.
doi:10.1016/j.cattod.2010.11.085

exposed microfacets as well [20–22]. Compared to the large amount of work conducted for Au/CeO_2(1 1 1), those on the supported catalysts involving CeO_2(1 1 0) and (1 0 0) are rather limited.

In this work, aiming at obtaining the basic understanding of some fundamental characteristics of supported Au/CeO_2 catalysts, we calculated the structural and electronic properties of Au trimer (Au_3) at CeO_2(1 1 1), (1 1 0) and (1 0 0) surfaces using DFT + U method. We considered only stoichiometric surfaces without defects, e.g. surface vacancies or steps, and they may provide simplified yet essential models for the related systems. Moreover, adsorption of O_2 molecule was also studied to shed some light on the performance of these systems in heterogeneous catalysis.

2. Calculations

We conducted density functional theory calculations corrected for on-site Coulomb interactions (DFT + U) in this work, where U = 5.0 eV was applied to the Ce 4*f* state [7,23,24]. The calculations have been performed within the generalized gradient approximation (GGA) using the VASP code [25,26]. The project-augmented-wave (PAW) method [27] was used to represent the core–valence interaction, and we treated the Ce (4*f*, 5s, 5p, 5d, 6 s), Au (5d, 6s, 6p) and O (2s, 2p) as valence states, while the remaining electrons were kept frozen as core states. The valence electronic states were expanded in plane-wave basis sets with energy cutoff at 350 eV.

The CeO_2(1 1 1), (1 1 0) and (1 0 0) surfaces were modeled as periodic slabs with three, five and four CeO_2 trilayers, respectively, and the vacuum between slabs was >10 Å. For CeO_2(1 1 1) and (1 0 0), a 3×3 expansion of the surface cell was utilized, and the CeO_2(1 1 0) was modeled by a 2×3 surface cell. These expansions largely remove the interactions among Au_3 clusters in neighboring surface cells. In all calculations, the triangular Au_3 cluster was adsorbed on one side of the slab only, and except those of the bottom layer of the slab, all the atoms were allowed to move in structural optimization (force threshold was 0.05 eV/Å). Due to the large size of the surface cells ($\sim 11 \times 11$ Å^2 for each surface cell), only $1 \times 1 \times 1$ k-point mesh was used. It needs to be mentioned that higher cutoff energy at 500 eV and $2 \times 2 \times 1$ k-point mesh were also tested, and the results regarding the relative stabilities of surface structures with localized electrons at different surface Ce were largely unchanged. For example, the most stable Au_3/CeO_2(1 1 1) configuration gives the stability of 0.18 eV better than the lest stable one when we used the cutoff energy at 350 eV and $1 \times 1 \times 1$ k-point mesh (see the next section, Table 1). It was then calculated to be 0.25 eV and 0.16 eV with 500 eV cutoff energy and $2 \times 2 \times 1$ k-point mesh, respectively.

The adsorption energies of Au_3 trimer (E_{ads}) at CeO_2 surfaces were measured by,

$$E_{ads} = -(E_{Au_3/CeO_2} - E_{Au_3} - E_{CeO_2})$$

Table 1
Calculated energetic and structural parameters of different Au_3/CeO_2 surfaces. E_{ads} is the estimated adsorption energy of the Au trimer and *d*[Ce–O] is average Ce–O distances of the reduced Ce with all the surrounding O.

	E_{ads} (eV)	*d*[Ce–O] (Å)	Figure
Au_3/CeO_2(111)	3.07	2.475	Fig. 2(a)
	3.00	2.467	Fig. 2(b)
	2.98	2.466	Fig. 2(c)
	2.94	2.461	Fig. 2(d)
	2.91	2.446	Fig. 2(e)
	2.89	2.453	Fig. 2(f)
Au_3/CeO_2(110)	3.28	2.433	Fig. 3(a)
	3.14	2.398	Fig. 3(b)
	3.13	2.419	Fig. 3(c)
	3.10	2.407	Fig. 3(d)
Au_3/CeO_2(100)	3.72	2.433	Fig. 3(f)
	3.42	2.446	Fig. 3(g)

where E_{Au_3/CeO_2} is the total energy of supported Au_3/CeO_2 system, and E_{Au_3} and E_{CeO_2} are the total energies of isolated Au_3 trimer in gas phase and the clean surface, respectively.

3. Results

The (1 1 1), (1 1 0) and (1 0 0) are three major facets of crystalline CeO_2. In Fig. 1(a)–(c), we present the bulk truncated structures of the three surfaces, respectively. It is known that bulk CeO_2 consists of 4-fold coordinated O and 8-fold coordinated Ce. We can see from these figures that the CeO_2(1 1 1) surface exposes coordinate-unsaturated 3(7)-fold O(Ce) (O_{3c} and Ce_{7c}), the CeO_2(1 1 0) exposes O_{3c} and Ce_{6c} and CeO_2(1 0 0) exposes O_{2c} and Ce_{6c}. One may note that CeO_2(1 1 1) has compact structures consisting of uninterrupted Ce–O bonding network all over the surface, while CeO_2(1 1 0) and (1 0 0) show rows of CeO_2 units separated along [00$\bar{1}$] and [0$\bar{1}\bar{1}$] directions, respectively. The above structural differences among these surfaces are consistent with the fact that the (1 1 1) facet was determined to be the most stable one, followed by (1 1 0) and (1 0 0) [7,28]. It needs to be mentioned that only the activities of these bulk truncated CeO_2 surfaces were compared in this work. Surfaces with low stabilities, such as CeO_2(1 1 0) and (1 0 0), may undergo reconstruction during preparation or application, which may affect their activities. However, these issues are beyond the scope of this paper.

3.1. Au_3/CeO_2(1 1 1)

For Au_3 adsorbed at CeO_2(1 1 1), different adsorption structures have been tested. In the energetically most stable one, two Au atoms of the trimer bind with two neighboring surface O_{3c}, respectively, and the other Au sits above these two Au atoms without forming any direct bond with the surface. From the calculated electronic configurations, we determined that there is one extra spin-polarized electron localized at a surface Ce upon Au_3 adsorption, turning this surface Ce^{4+} cation into Ce^{3+}. Interestingly, we

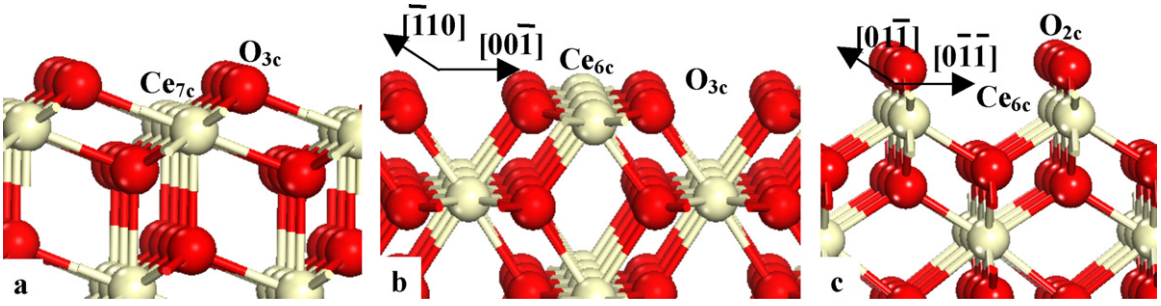

Fig. 1. Bulk truncated structures (side view) of CeO_2 (a) (1 1 1), (b) (1 1 0) and (c) (1 0 0) surfaces. Ce is in white and O in red. This notation is used throughout the paper. (For interpretation of references to color in this figure legend, the reader is referred to the web version of this article.)

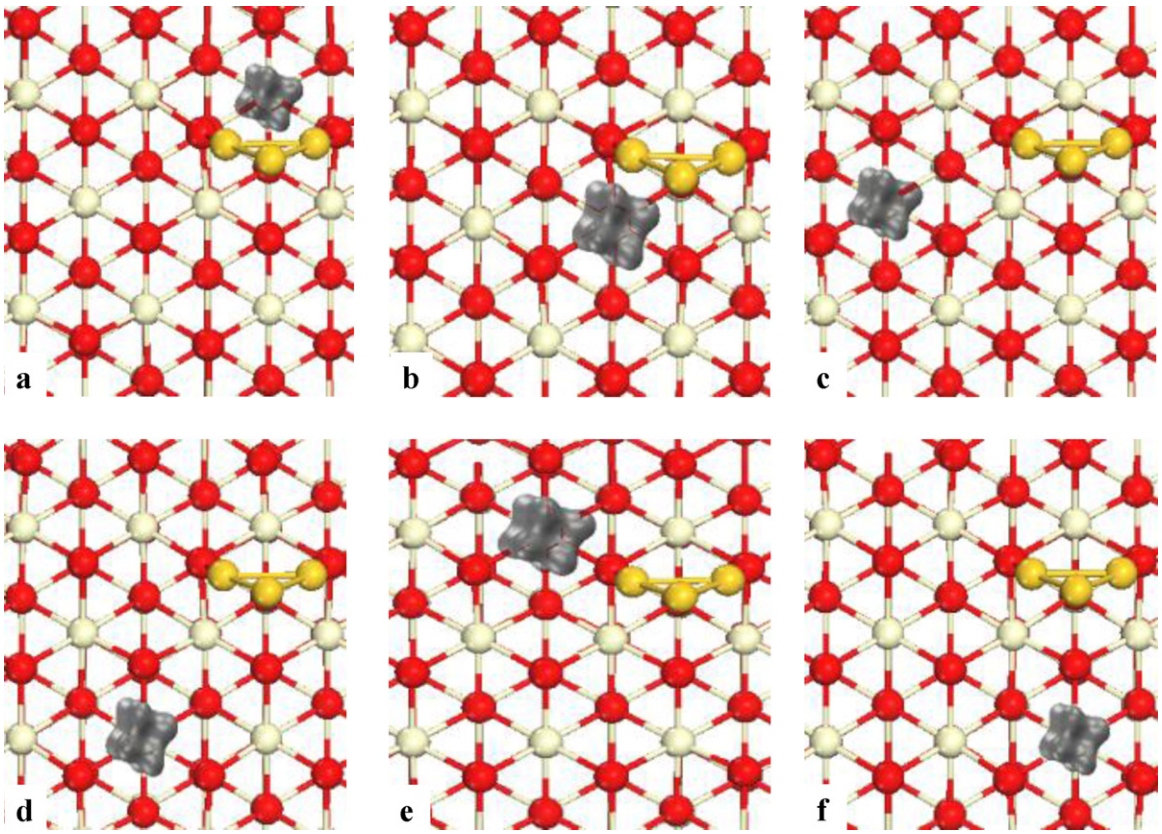

Fig. 2. Calculated structures (top view) of the Au_3 (in gold) adsorbed $CeO_2(1\,1\,1)$ surfaces. The isosurface of calculated charge density of the localized 4*f* electron at different positions is in gray. This notation is used throughout the paper. (For interpretation of references to color in this figure legend, the reader is referred to the web version of this article.)

found that the localized electron may occur at 6 different surface Ce around the adsorbed Au_3 trimer. In Fig. 2(a)–(f), we illustrate the surfaces with the localized electron at these different positions in the order of decreasing stabilities. In Table 1, we also list the estimated Au_3 adsorption energies corresponding to the different localization configurations. For the energetically most favorable structure, the single electron is localized at the Ce_{7c} that binds to both the O_{3c} directly interacting with the Au_3. It is clear that this is also the surface Ce_{7c} closest to the adsorbed Au_3 trimer. For other less favorable structures, the localized electron stays at the Ce_{7c} not so close to the adsorbed Au_3, and in general, the stability of adsorbed Au_3 decreases with respect to the increase of its distance to the localized electron. Nevertheless, as one can see from Table 1, these different structures give rather close adsorption energies, which range from 2.89 to 3.07 eV.

3.2. $Au_3/CeO_2(1\,1\,0)$

As we have shown in Fig. 1(b), the bulk truncated $CeO_2(1\,1\,0)$ surface exposes O_{3c} and Ce_{6c} at discrete CeO_2 rows. From calculations, we determined that Au_3 at $CeO_2(1\,1\,0)$ prefers the upright configuration: two Au atoms of the trimer bind with two O_{3c}, respectively, at the same side of one CeO_2 row, while the other Au atom forms no direct bond with the surface (see Fig. 3). We also determined that there is one extra electron localized at the surface Ce_{6c} upon Au_3 adsorption. Moreover, the localized electron was found to be able to occur at different Ce_{6c}. As one can see from Fig. 3 and Table 1, for the energetically most favorable $Au_3/CeO_2(1\,1\,0)$ structure (Fig. 3(a)), the localized electron occurs at the Ce_{6c} right beside the adsorbed Au_3. It gives the Au_3 adsorption energy of 3.28 eV, which is ~0.2 eV higher than that of the most stable Au_3 at $CeO_2(1\,1\,1)$. For the configuration with the second highest stability (Fig. 3(b)), the localized electron occurs at the Ce_{6c} that shares only one O_{3c} with the adsorbed Au_3, and the corresponding Au_3 adsorption energy was estimated to be 3.14 eV. In addition, the localized electron can also occur at Ce_{6c} of the neighboring CeO_2 row that has almost no direct interaction with the adsorbed Au_3 (Fig. 3(c) and (d)), and the adsorption energies were calculated to be 3.13 and 3.10 eV.

3.3. $Au_3/CeO_2(1\,0\,0)$

As we have discussed early, the $CeO_2(1\,0\,0)$ surface exposes O_{2c} arranged continuously along the $[01\bar{1}]$ direction while such O_{2c} rows are separated along the $[0\bar{1}\bar{1}]$ direction (see Fig. 1(c)). Through calculations, we determined that the Au_3 trimer adsorbs at $CeO_2(1\,0\,0)$ with two Au atoms bonding with two neighboring O_{2c} along $[01\bar{1}]$, respectively, while the other Au on the top again has no direct bond with surface atoms (see Fig. 3).

Similar to what occurs at the other two CeO_2 surfaces, Au_3 adsorption at $CeO_2(1\,0\,0)$ also induces charge redistribution at the interface, and as the result, there forms one localized electron at a top surface Ce_{6c}. However, Ce_{6c} at only two different positions with respect to the adsorbed Au_3 trimer were capable of being reduced. As one can see from Fig. 3, the Ce_{6c} right below the Au_3, either at the same or the row next to it, can be the site where the localized electron occurs. In addition, it can be seen from the data listed in Table 1 that the former gives Au_3 adsorption energy of 3.72 eV and the latter 3.42 eV, which are significantly higher than those at the other two surfaces.

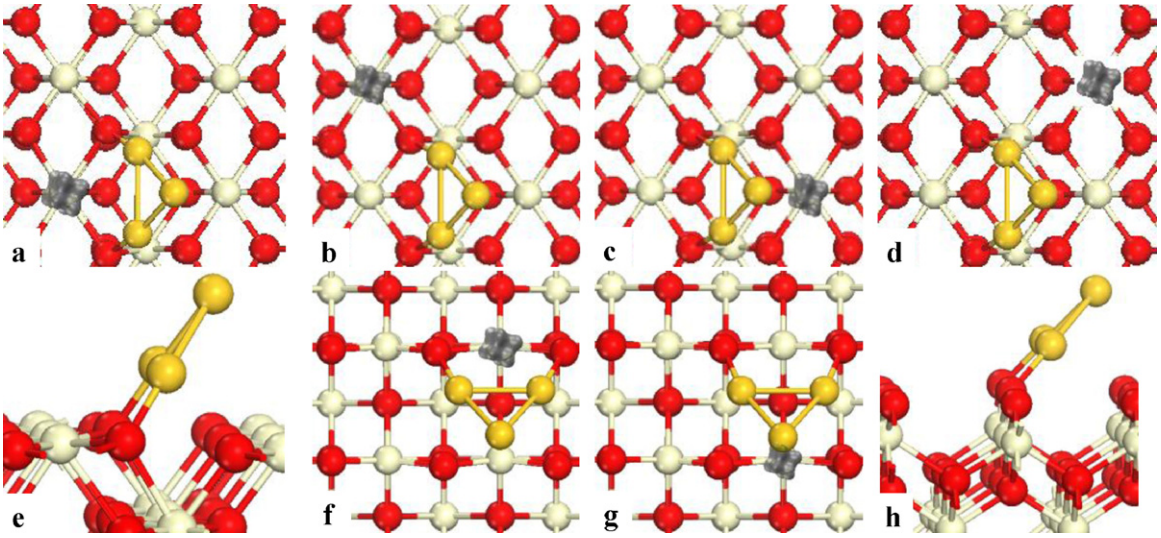

Fig. 3. Calculated structures of the Au_3 adsorbed $CeO_2(1\,1\,0)$ ((a)–(d) top view, (e) side view) and $CeO_2(1\,0\,0)$ ((f) and (g) top view, (h) side view) surfaces with localized 4*f* electron at different positions.

3.4. O_2 adsorption

For a wide range of heterogeneous catalytic reactions, the activation of oxygen species is a key step [29]. With respect to the CeO_2 related materials, active oxygen species at the surface is of particular importance since it is not only involved in many catalytic oxidation reactions and also directly related to other processes such as oxygen storage and formation/healing of oxygen vacancy [30]. In the current work, preliminary studies of the catalytic performance of the systems containing metal nanoclusters supported at CeO_2 surfaces were conducted by calculating the O_2 adsorption at the various Au_3/CeO_2 surfaces reported above. It needs to be mentioned that only O_2 adsorption at the CeO_2 substrate was considered in this work. This is because that (i) the adsorbed Au_3 trimer is indeed very small and our testing calculations showed that O_2 cannot strongly adsorb on it; and (ii) it has already been determined in our recent work that partially reduced $CeO_2(1\,1\,1)$ surface may donate electrons to O_2 and promote its adsorption [31].

The adsorption of single O_2 molecule at the $CeO_2(1\,1\,1)$, $(1\,1\,0)$ and $(1\,0\,0)$ surfaces, both clean and with adsorbed Au_3 trimer, was systematically calculated. Similar to the results reported in early studies, there was no adsorption at the clean surfaces. In addition, at $Au_3/CeO_2(1\,1\,1)$ and $Au_3/CeO_2(1\,0\,0)$, there was no O_2 adsorption obtained at various Ce^{3+} sites either, even though the O_2 molecule was placed quite close to these sites at the beginning of the optimization (<2.5 Å).

By contrast, we located various O_2 adsorption configurations at $Au_3/CeO_2(1\,1\,0)$. As we have explained in Section 3.2, there are four different surface Ce_{6c} around the adsorbed Au_3 cluster that can be possibly reduced to Ce^{3+} by the cluster. From calculations, we determined that O_2 molecule can adsorb at these four different Ce_{6c} rather strongly with two O binding to this single Ce in a chelating bidentate configuration (see Fig. 4). In Table 2, we list the structural parameters of the O_2 at these different sites together with the corresponding estimated adsorption energies. One can see that the adsorbed O_2 at the different sites have similar structures, and the O–O bond distance and the average O–Ce bond length were measured to be ~1.34 and ~2.43 Å, respectively. From the calculated adsorption energies, we can also see that O_2 adsorption at the two Ce_{6c} that are the second neighbor to the adsorbed Au_3 has relatively higher stabilities. As we have listed in Table 2, they both give the O_2 adsorption energy of ~0.7 eV with respect to the most stable $Au_3/CeO_2(1\,1\,0)$ slab (Fig. 3(a)). From calculations, we also determined that there occurs one spin electron in each adsorption system and it is localized at the adsorbed O_2. By plotting the space distribution of this spin electron, we can see that it actually stays in the anti-bonding $2\pi^*$ orbital (see Fig. 4(e)). The above results regarding the geometric, energetic and electronic properties of the adsorbed O_2 clearly suggest that it actually forms an O_2^- species at these sites. Moreover, by analyzing the charge distribution at surface Ce_{6c}, we found that they are all Ce^{4+}, indicating that the O_2^- species occurs through reduction of adsorbed O_2 by surface Ce^{3+}. Or, one can expect that it is the adsorbed Au_3 cluster that reduces adsorbed O_2, indirectly, via the CeO_2 surface that they both interact with.

It needs to be mentioned that the final O_2 adsorption configuration is not dependent on the initial structures of the $Au_3/CeO_2(1\,1\,0)$ substrate or the initial positions of the adsorbed O_2. In other words, no matter where the localized electron stays at the $(1\,1\,0)$ surface or which Ce_{6c} the O_2 is initially located at, the optimization always gives adsorption structures with the localized electron being transferred to the adsorbed O_2.

Besides the single O_2 adsorption, stable configurations with two O_2 at different surface Ce_{6c} can be also located. For example, as we have presented in Fig. 4(f), the co-adsorption of two O_2 at two Ce_{6c} on the two sides of the adsorbed Au_3 trimer can give average adsorption energy of 0.43 eV per molecule. According to the electronic analysis, each O_2 now contains a spin-polarized electron. Interestingly, the Bader charge analysis also showed that the adsorbed Au_3 trimer is now positively charged with 0.42 e, which is relatively larger than those in the systems with a single adsorbed O_2 (see Table 2).

Table 2
Calculated energetic, structural and electronic parameters of adsorbed O_2 at the $Au_3/CeO_2(1\,1\,0)$ surface. E_{ad} is the adsorption energy of O_2 and $\delta(Au_3)$ is the calculated Bader charge of the trimer (relative to that of gas-phase one). d[O–O] is the interatomic distance of adsorbed O_2. d[O–Ce] is the average Ce–O distances of the O_2 with the Ce.

Figure	Fig. 4(a)	Fig. 4(b)	Fig. 4(c)	Fig. 4(d)	Fig. 4(f)
E_{ad} (eV)	0.69	0.69	0.44	0.48	0.85 (0.43/O_2)
$\delta(Au_3)$	0.31 e	0.32 e	0.38 e	0.32 e	0.42 e
d[O–O] (Å)	1.339	1.339	1.345	1.340	1.307
d[O–Ce] (Å)	2.432	2.428	2.421	2.442	2.589

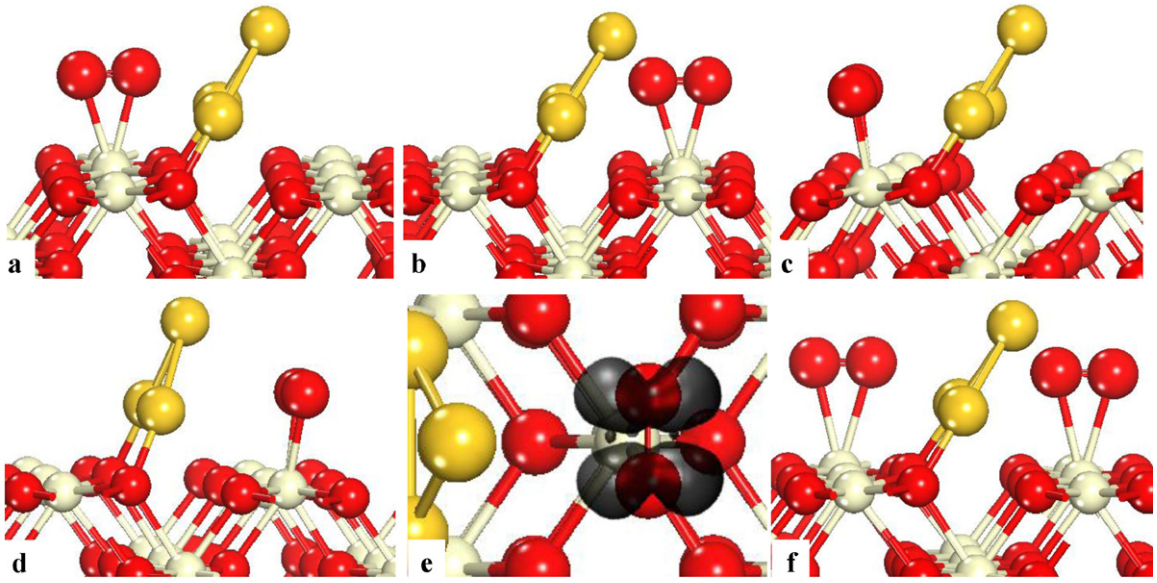

Fig. 4. Calculated structures ((a)–(d) side view) of O_2 adsorption at different sites of $Au_3/CeO_2(1\,1\,0)$ surface. The isosurface (in semi-transparent black) ((e) top view) for the charge density of spin electron in the adsorption system shown in (d). Calculated structures ((f), side view) of the adsorption of two O_2 beside Au_3.

4. Discussion

Surface reduction–oxidation has long been expected to be a key property for reducible metal oxides, such as titanium [32], cobalt and cerium oxides [33], which are highly active as catalysts or catalytic supports. In this work, we have systematically calculated the supported catalysts with small Au cluster at various CeO_2 surfaces and found that reduction–oxidation does occur in the interacting systems. In particular, by performing Bader charge analysis, we were able to determine that the adsorbed Au_3 trimer is now positively charged and one surface Ce cation is significantly less positive compared to others or those at clean CeO_2 surfaces. From the plotted charge distribution of the spin-polarized electron (see the shape of the isosurface in Figs. 2 and 3), we were able to tell that one excess electron exclusively stays in the 4*f* orbital of this partially reduced Ce, which is empty for Ce^{4+} cations. These results clearly suggest that it is the adsorbed Au_3 that reduces the CeO_2 supports by charge donation to the empty 4*f* orbital of one surface Ce^{4+} cation and turing it into Ce^{3+}.

It is also interesting to note that such Ce^{3+} can actually occur at different positions with respect to the adsorbed Au_3 trimer, i.e. there are six, four and two different surface Ce capable of taking the single excess electron at $CeO_2(1\,1\,1)$, $(1\,1\,0)$ and $(1\,0\,0)$ (see Figs. 2 and 3). Similar results were obtained at $CeO_2(1\,1\,1)$ reduced by the occurrence of surface O vacancy. In the recent theoretical work by us and several other groups, it has been shown that the two electrons left by a missing O have multiple distribution configurations at the surface [31,34–36]. It has also been pointed that where the two electrons stay and the relative stabilities are largely determined by surface relaxation caused by the O vacancy, and the energetically most favorable distribution configuration always corresponds to the one with each electron at a second-nearest Ce with respect to the vacancy.

In the current work, the existence of multi-configurations for the single electron to distribute at various Au_3 adsorbed CeO_2 surfaces can be also explained from surface structures. Upon adsorption, the Au_3 trimer would cause structural relaxation to the surface atoms, especially those close to the adsorption site. From the chemical point of view, we can also expect that when the surface O atoms form new bonds with adsorbed Au_3, the original surface bonds between Ce and O would be distorted accordingly. By comparing the optimized structures of the various surfaces containing supported Au_3 trimer, we found that they have different surface relaxation configurations, and each gives a surface Ce that has the longest average Ce–O bonds with neighboring lattice O. Remarkably, this corresponding Ce is just the one that is reduced to Ce^{3+}, i.e. where the electron is localized in its 4*f* orbital. For example, at $CeO_2(1\,1\,1)$, upon Au_3 adsorption, there exist six different Ce that can be possibly reduced to Ce^{3+}. In the system with the localized electron occurring at the Ce that shares two surface O_{3c} with the Au_3 trimer (see Fig. 2(a)), the average Ce–O bonds for this Ce, which is 2.344 Å at the stoichiometric surface presented in Fig. 1(a), is measured to be 2.475 Å (all seven bonds are counted). In particular, the two Ce–O bonds with the O binding directly with the Au_3 increase to as long as 2.607 Å and 2.598 Å, respectively. On the other hand, for the lest stable configuration with the corresponding Au_3 adsorption energy of 2.89 eV only, the localized electron occurs at one Ce far away from the adsorbed Au_3 (see Fig. 2(f)). In this case, the average Ce–O bond length for this Ce is measured to be 2.453 Å; while the average Ce–O distance of the Ce that takes the localized electron in the configuration shown in Fig. 2(a) now decreases to 2.363 Å. Similar results can be also obtained in the cases of Au_3 supported at $CeO_2(1\,1\,0)$ and $(1\,0\,0)$.

Surface structural relaxation not only determines where the localized electron occurs, but also affects the relative stabilities of the surfaces with the localized electron at various positions and even how many different localization configurations may exist at these CeO_2 surfaces. From the results presented in Figs. 2 and 3 and Table 1, we can generally see that at various CeO_2 surfaces, the adsorption configurations with the localized electron occurring rather close to the adsorbed Au_3 trimer usually give higher stabilities. This is clearly due to the fact that the adsorbed Au_3 trimer tends to cause significant disturbance to the support only within the area in close interaction with the adsorbate, while the surface relaxation rather far away from the adsorption site would be unfavorable to occur. Moreover, at the very compact $CeO_2(1\,1\,1)$ where the surface O and Ce atoms have close and continuous interactions with each other, the structural disturbance brought by the incoming Au_3 trimer could affect more extensively, and therefore, we were able to determine quite a lot configurations with the localized electron at different positions. By contrast, for the less compact $CeO_2(1\,1\,0)$ and $(1\,0\,0)$ surfaces, the surface Ce and O atoms form rows of CeO_2 struc-

tures, while neighboring rows are widely separated. This indicates that the disturbance brought by the Au_3 adsorbate would be heavily blocked by the row gaps and have limited effect on the surface. Accordingly, the possible surface relaxation would be restricted within the area very close to the adsorption site. Therefore, we only determined 4 and 2 different positions for the localized electron to possibly occur at the CeO_2(1 1 0) and (1 0 0) surfaces, respectively.

The interaction between O_2 and CeO_2 surfaces is of particular interest since it is directly related to the catalytic performance of CeO_2 as the oxygen buffer in three-way-catalysts [37]. In a recent work, we studied the CeO_2(1 1 1) with single surface O vacancy and showed that the second-nearest Ce around a subsurface O vacancy would be the most favorable one for a localized electron to stay and such localized electron can promote O_2 adsorption (E_{ad} = ~0.4 eV) by transferring to it and making it a O_2^- [31,36]. In addition, the adsorption also causes significant structural relaxation: one top surface O_{3c} originally binding with that second-nearest Ce moves further toward the O vacancy so that the incoming O_2 can insert in-between and comfortably bind with that Ce.

In the current work, O_2 adsorption was systematically calculated at the surface Ce of various CeO_2 surfaces reduced by pre-adsorbed Au_3. Although all these surfaces can provide exposed Ce^{3+} cations, only those at CeO_2(1 1 0) are able to hold the O_2 with rather high adsorption energy and activate it into O_2^- through charge transfer. By contrast, no adsorption configuration was determined at the CeO_2(1 1 1) or (1 0 0) surfaces. By simply looking at the surface structures of the different systems, one can notice that the exposed surface Ce of (1 1 1) and (1 0 0) are both shielded by neighboring lattice O from all around, while that of (1 1 0) only binds with lattice O in the same plane and below in the bulk and gives obvious dangling bond pointing toward the vacuum. Accordingly, O_2 cannot adsorb at surface Ce of CeO_2(1 1 1) or (1 0 0) just because that the uniformly surrounding lattice O, especially those above the surface plane, heavily repel the incoming O_2 and prevent the formation of strong Ce–O_2 interaction. For CeO_2(1 1 0), since there is no such protruding lattice O around the exposed Ce, the O_2 would be able to comfortably approach such site, and by taking the extra electron donated by Au_3 it forms a negatively charged O_2^- that can sit at the Ce^{4+} cation with reasonable stability mainly through strong electrostatic interaction. These results suggest that the activity of CeO_2 support in heterogeneous catalysts, especially in the cases involving direct interaction between reactants and the support, could be orientation dependant, and its (1 1 0) facet could be of particular importance. Moreover, as we have shown by calculating adsorption of multiple O_2 molecules at the Au_3/CeO_2(1 1 0), more electrons are able to transfer from the Au nanoparticle to them to promote their adsorption and activation. Then, it can be proposed that CeO_2(1 1 0) may act as 'smart' oxide support and electron buffer capable of tuning the charge transfer on demand between adsorbates and metal clusters, which are not in direct contact. It should be emphasized that in this work, the activities of supported Au catalysts with stoichiometric CeO_2(1 1 1), (1 1 0) and (1 0 0) surfaces as the supports were tested by calculating O_2 adsorption. Moderate adsorption strength was obtained at the Au_3/CeO_2(1 1 0) only. However, under different conditions (for example, very high temperature) or when reactants other than O_2 are involved, their activities as the supports may be different from what we have determined here [5,38].

5. Conclusion

In this work, by performing systematic DFT calculations, we have studied the supported rare earth catalysts containing small Au nanoparticle at various CeO_2 surfaces. The results have shown that the Au nanoparticle at CeO_2(1 1 1), (1 1 0) and (1 0 0) has strong interaction with the support and can reduce the surface through electron donation to a surface Ce near the adsorption site. The transferred electron at the Ce was found to exclusively stay in its 4*f* orbital. Moreover, for all these different CeO_2 surfaces, the adsorption of Au nanoparticle can cause structural relaxation at the support, and corresponding to different relaxation configurations, the localized electron may occur at different surface Ce. O_2 adsorption was tested to provide insight into the catalytic activities of these supported systems. It was determined that only at CeO_2(1 1 0), the surface Ce of which contain obvious dangling bonds, the O_2 can adsorb with high stability and be activated to an O_2^- species by taking the localized electron from surface Ce. These results exhibit some unique properties of rare earth catalysts and may help understand their catalytic performance.

Acknowledgements

The authors thank financial support from National Basic Research Program (2010CB732300), National Natural Science Foundation (21073060) of China and Shanghai Rising-Star Program (09QA1401300).

References

[1] J.C. Fierro-Gonzalez, B.C. Gates, J. Phys. Chem. B 108 (2004) 16999.
[2] J.C. Fierro-Gonzalez, B.C. Gates, Catal. Today 122 (2007) 201.
[3] Q. Fu, H. Saltsburg, M. Flytzani-Stephanopoulos, Science 301 (2003) 935.
[4] R. Burch, Phys. Chem. Chem. Phys. 8 (2006) 5483.
[5] J.A. Rodriguez, P. Liu, J. Hrbek, J. Evans, M. Perez, Angew. Chem. Int. Ed. 46 (2007) 1329.
[6] M. Nolan, S.C. Parker, G.W. Watson, Phys. Chem. Chem. Phys. 8 (2006) 216.
[7] M. Nolan, S. Grigoleit, D.C. Sayle, S.C. Parker, G.W. Watson, Surf. Sci. 576 (2005) 217.
[8] A. Haruta, Chem. Rec. 3 (2003) 75.
[9] C.J. Zhang, A. Michaelides, D.A. King, S.J. Jenkins, J. Am. Chem. Soc. 132 (2010) 2175.
[10] L.M. Molina, J.A. Alonso, J. Phys. Chem. C 111 (2007) 6668.
[11] H.F. Wang, X.Q. Gong, Y.L. Guo, Y. Guo, G.Z. Lu, P. Hu, J. Phys. Chem. C 113 (2009) 6124.
[12] Z.P. Liu, S.J. Jenkins, D.A. King, Phys. Rev. Lett. 94 (2005) 4.
[13] M. Skoda, M. Cabala, I. Matolinova, K.C. Prince, T. Skala, F. Sutara, K. Veltruska, V. Matolin, J. Chem. Phys. 130 (2009) 034703.
[14] N.C. Hernandez, R. Grau-Crespo, N.H. de Leeuw, J.F. Sanz, Phys. Chem. Chem. Phys. 11 (2009) 5246.
[15] Y. Chen, P. Hu, M.H. Lee, H.F. Wang, Surf. Sci. 602 (2008) 1736.
[16] C.J. Zhang, A. Michaelides, D.A. King, S.J. Jenkins, J. Phys. Chem. C 113 (2009) 6411.
[17] C.J. Weststrate, R. Westerstrom, E. Lundgren, A. Mikkelsen, J.N. Andersen, J. Phys. Chem. C 113 (2009) 724.
[18] M. Baron, O. Bondarchuk, D. Stacchiola, S. Shaikhutdinov, H.J. Freund, J. Phys. Chem. C 113 (2009) 6042.
[19] M.F. Camellone, S. Fabris, J. Am. Chem. Soc. 131 (2009) 10473.
[20] H. Norenberg, J.H. Harding, Surf. Sci. 477 (2001) 17.
[21] H. Norenberg, G.A.D. Briggs, Surf. Sci. 433 (1999) 127.
[22] H. Norenberg, G.A.D. Briggs, Surf. Sci. 424 (1999) 352.
[23] M. Nolan, S.C. Parker, G.W. Watson, Surf. Sci. 595 (2005) 223.
[24] M. Nolan, S.C. Parker, G.W. Watson, J. Phys. Chem. B 110 (2006) 2256.
[25] G. Kress, Comput. Mater. Sci. 6 (1996) 15.
[26] G. Kress, Phys. Rev. B 49 (1994) 14251.
[27] P.E. Blochl, Phys. Rev. B 50 (1994) 17953.
[28] J. Conesa, Surf. Sci. 339 (1995) 337.
[29] L.M. Liu, B. McAllister, H.Q. Ye, P. Hu, J. Am. Chem. Soc. 128 (2006) 4017.
[30] M. Nolan, J. Chem. Phys. 130 (2009) 144702.
[31] H.Y. Li, H.F. Wang, X.Q. Gong, Y.L. Guo, Y. Guo, G.Z. Lu, P. Hu, Phys. Rev. B 79 (2009) 193401.
[32] S. Chretien, H. Metiu, J. Chem. Phys. 129 (2008) 16.
[33] L.F. Liotta, G. Di Carlo, G. Pantaleo, A.M. Venezia, G. Deganello, Appl. Catal. B: Environ. 66 (2006) 217.
[34] C.J. Zhang, A. Michaelides, D.A. King, S.J. Jenkins, Phys. Rev. B 79 (2009) 075433.
[35] M.V. Ganduglia-Pirovano, J.L.F. Da Silva, J. Sauer, Phys. Rev. Lett. 102 (2009) 026101.
[36] J.C. Conesa, Catal. Today 143 (2009) 315.
[37] F. Esch, S. Fabris, L. Zhou, T. Montini, C. Africh, P. Fornasiero, G. Comelli, R. Rosei, Science 309 (2005) 752.
[38] J.A. Rodriguez, P. Liu, M. Perez, G. Liu, J. Hrbek, J. Phys. Chem. A 114 (2010) 3802.